IJE TRANSACTIONS A: Basics Vol. 35, No. 07, (July 2022) 1330-1342

International Journal of Engineering

Journal Homepage: www.ije.ir

Jensen-Shannon Divergence of Two Eddy Current Distributions Induced by Circular and Fractal Koch Excitation Coils

C. Guolong*, C. Zheng, J. Wuyin

School of Mechanical and Electrical Engineering, Lanzhou university of technology, Lanzhou, China

P A P E R I N F O

Paper history:
Received 08 March 2022
Received in revised form 28 March 202
Accepted 09 April 2022

Keywords:
Jensen-Shannon Divergence
Fractal Geometry
Excitation Coil
Eddy Current Testing
Differential Pickup Probes
Entropy

A B S T R A C T

Eddy current distribution is important to the performance of planar eddy current probes. In this paper, the Jensen-Shannon divergences of tangential intersection angle spectrum and radial direction energy spectrum were proposed to evaluate the difference between eddy current distributions generated by circular and fractal Koch excitation coils. By the simulation for the circular and Koch shape excitation coils, it works out that the difference of the eddy current distributions between the two kinds of coils becomes larger and larger with an increase in the values of the two Jensen-Shannon divergences. At the same time, the correlation between the change of Jensen-Shannon divergence and the detectability of the short crack in the special direction was discussed through simulation and experiment results. It is found that, relative to the crack in 0° direction, the detectability of the Koch and circular differential pickup probes to the crack in 90° direction has a correlation with the Jensen-Shannon divergence of tangential intersection angle spectrum. The width of each signal generated by the two probes has a correlation with the Jensen-Shannon divergence of radial direction energy spectrum.

***doi**: 10.5829/ije.2022.35.07a.12*

1. INTRODUCTION

As one of the common nondestructive methods, eddy current (EC) testing (ECT) based on the principle of electromagnetic induction has the advantages of non-contact, using without coupling agent and fast testing speed [1]. According to these advantages, it is widely used to detect defects on the surface or subsurface of conductors. In the process of ECT, EC probes are taken as the source of information to obtain some physical properties of tested objects. When detecting the defects in components, EC probes determine the performance of the whole ECT system. Furthermore, they have an impact on the accuracy of subsequent quantitative evaluation to defects.

Recently, the research of EC probes focuses on improving the structure. Traditional three-dimensional rigid EC probes can test metal parts with simple geometry structure of the surface, but they are not able to reach some tested portion thoroughly for the components with complex structure [2,3]. In view of this, two-dimensional planar flexible EC probes have been proposed. This category of probe can be manufactured easily, folded and touch the tested surface furthest [4,5]. Therefore, it overcomes the disadvantage of three-dimensional probe. Aimed at the design of flexible or planar EC probe, various coil structures have been proposed like meandering winding magnetometer structure [6], rosette structure [7,8], rectangular structures [9,10], circular spiral structure [11,12], floral-shape structure [13], butterfly-shape structure [14], Koch-shape structure [15,16]. In addition, some special structures and configuration methods were put forward for the inspection of flaws. Xie et al. [17] used a novel flexible EC probe to detect small cracks of materials with complex geometry. Zhang et al. [18] designed a flexible EC probe whose coils are arranged as a parallel and stagger method for the inspection of last stage blades of a steam turbine. Aouf et al. [19] proposed a multi-probe system composed of three differential probes which are arranged within a specific configuration. This kind of configuration has efficiency and robustness in the

*Corresponding Author Institutional Email: cgl20061273@126.com
(C. Guolong)

Please cite this article as: C. Guolong, C. Zheng, J. Wuyin, Jensen-Shannon Divergence of Two Eddy Current Distributions Induced by Circular and Fractal Koch Excitation Coils, ***International Journal of Engineering, Transactions A: Basics,*** Vol. 35, No. 07, (2022) 1330-1342

detection of cracks. Chen et al. [20] designed a double-layer differential planar coil to detect surface defects, and has high sensitivity even under large lift-off affection. Fan et al. [21] proposed a flexible EC probe based on a TMR probe, this kind of probe can quantitatively monitor the cracks below 3-5mm of material surface. Zhang et al. [22] presented a planar EC probe whose excitation coils were energized by three-phase currents. This excitation method is sensitive to defects of any orientations.

Nevertheless, flexible EC probes have fewer coil turns than those of three-dimensional rigid probes. Also, EC distributions induced by coils determine the interaction effect between ECs and cracks. Therefore, the suitable coil structure and configuration play key roles in flexible EC probes [23], and it is necessary to evaluate the EC distributions for the sake of designing coil structure reasonably. Zhang et al. [24] firstly analyzed EC distributions of line, circle and fractal Koch coils through information entropy. Subsequently, Chen et al. [25, 26] put forward information entropy based on tangential intersection angle spectrum (TIAS) and radial direction energy spectrum (RDES). In Chen's method, the TIAS can evaluate EC distributions from their diversity in directions, and the RDES can reflect the concentration degree of EC distributions under excitation coils. However, the information entropy cannot evaluate the difference between EC distributions induced by two different coils. To solve this problem, the relative entropy and cross entropy were proposed for the evaluation of EC distributions induced by two different coils [23]. Whereas, the relative entropy and cross entropy are asymmetric for two probability distributions, and cannot evaluate the difference of them accurately. Hence, in this study, Jensen-Shannon (JS) divergences of TIAS and RDES are proposed to evaluate the EC distributions between two kinds of coils. Taken as an example, the EC distributions induced by a circular coil and a Koch coil are studied. In addition, simulations and experiments of circular and Koch differential pickup probes are carried out respectively to research the correlation between the performance of the two probes and the JS divergences.

2. METHODOLOGY

2. 1. Basic Principle of JS Divergence According to Jensen inequation and Shannon entropy, Lin proposed a new measure, JS divergence, to evaluate several probability distributions [27]. As the increment of entropy, JS divergence is commonly used to evaluate the similarity between two probability distributions. It can be formulated as Equation (1):

$$JS(P\|Q)=\frac{1}{2}KL(P\|\frac{P+Q}{2})+\frac{1}{2}KL(Q\|\frac{P+Q}{2}) \quad (1)$$

where P and Q are two different probability distributions, respectively. $KL(P\|Q)$ represents Kullback-Leibler (KL) divergence namely the relative entropy, and it can be expressed as Equation (2):

$$KL(P\|Q)=E_p \log\frac{P}{Q} \quad (2)$$

The range of JS divergence is [0,1]. When its value increases from 0 to 1, it means that the similarity of P and Q will decrease. Otherwise, JS divergence overcomes the asymmetry of KL divergence for the evaluation between two probability distributions.

2. 2. JS Divergence of TIAS In order to evaluate the difference of EC distributions induced by two kinds of excitation coils from the view of the richness of TIA, the JS divergences of TIASs are worked out via four steps as shown in Figure 1.

(1) As is shown in Figure 1(a), sample points are distributed uniformly and with the same interval. The energy of the EC at every point is $J^2(x,y)=J_x^2(x,y)+J_y^2(x,y)$.

(2) The intersection angle θ of every point is the angle between AB line and EC vector J in Figure 1(b). Thereinto, AB line is perpendicular to AO line. Thus, the intersection angle can be expressed as Equation (3):

$$\theta=<\overrightarrow{AB},\vec{J}>=\arccos\frac{yJ_x-xJ_y}{\sqrt{x^2+y^2}\sqrt{J_x^2+J_y^2}},\ \text{for } x^2+y^2\neq 0 \quad (3)$$

In the expression, $\theta=\begin{cases}\theta & \text{if } \theta\le 90°\\ 180°-\theta & \text{else}\end{cases}$.

(3) The range $[0°,90°]$ is equally divided into m parts. The size of every angle interval is $\frac{90°}{m}$. Therefore, the energy of EC in every angle interval can be calculated by Equation (4):

$$J_p^2(k)=\sum J^2_{90°(k-1)/m\le\theta_k\le 90°k/m}(x,y) \quad (4)$$

where θ_k is the intersection angle belonging to k-th angle interval. Hence, the TIAS is calculated by Equation (5):

$$P(k)=\frac{J_p^2(k)}{\sum_{k=1}^{m}J_p^2(k)} \quad (5)$$

It is known from the above that can characterize the TIAS under a specific EC distribution. Via the same approach, $Q(k)=\frac{J_q^2(k)}{\sum_{k=1}^{m}J_q^2(k)}$ is used to characterize the TIAS under another kind of EC distribution. In Figure 1c, there are

schematic diagrams of TIASs under two different kinds of EC distributions.

(4) Based on the TIASs, the JS divergence is further calculated by Equation (6).

$$JS(P(k)\,||\,Q(k))=\frac{1}{2}KL(P(k)\,||\,\frac{P(k)+Q(k)}{2})+\frac{1}{2}KL(Q(k)\,||\,\frac{P(k)+Q(k)}{2}) \quad (6)$$

2. 3. JS Divergence of RDES In order to evaluate the difference of EC distributions induced by two kinds of excitation coils from the view of distribution proportion of RDE in annuluses, the JS divergences of RDESs are worked out via four steps as follows.

(1) The method to set sample points is the same as section 2.2.

(2) As can be seen from Figures 2(a) and 2(b), the sample space includes annuluses whose widths are same as each other. The radius of the circle located in the center has the same width h for every annulus.

(3) The EC energy in every annulus can be expressed as Equation (7):

$$J_s^2(j)=\sum J_{h(j-1)\le r_j\le hj}^2(x,y) \quad (7)$$

where r_j denotes the distance between the sample point in the j-th (i=1,2,3···n) annulus and origin.

The total EC energy in all annuluses is $J_s^2=\sum_{j=1}^{n} J_{0\le r_j\le hn}^2(x,y)$.

Thus, the RDES can be calculated by Equation (8):

$$S(j)=\frac{J_s^2(j)}{\sum_{j=1}^{n} J_s^2(j)} \quad (8)$$

S(j) can characterize the RDES under one EC distribution. Correspondingly, $T(j)=\frac{J_t^2(j)}{\sum_{j=1}^{n} J_t^2(j)}$ can be used to describe the RDES under another EC distribution in the same way. Figure 2(c) displays the RDESs about two different EC distributions.

(4) Then, by Equation (9), the JS divergence based on RDES can be obtained to evaluate the difference between two EC distributions.

$$JS(S(j)\,||\,T(j))=\frac{1}{2}KL(S(j)\,||\,\frac{S(j)+T(j)}{2})+\frac{1}{2}KL(T(j)\,||\,\frac{S(j)+T(j)}{2}) \quad (9)$$

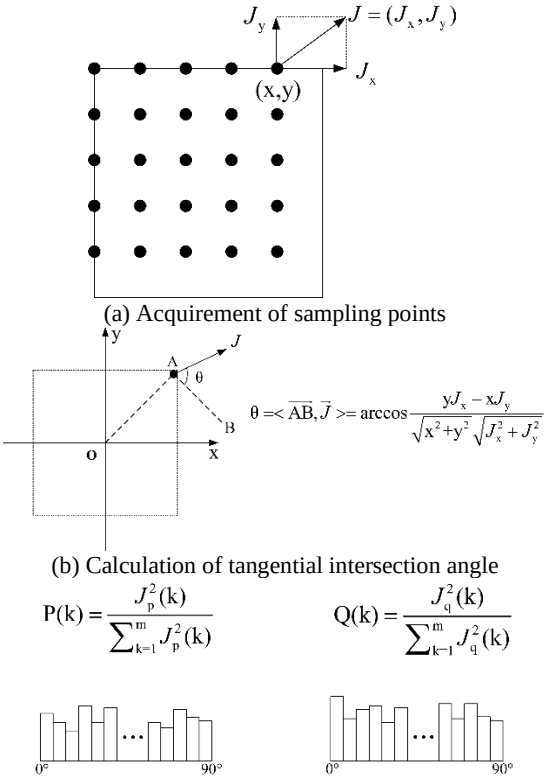

(a) Acquirement of sampling points

(b) Calculation of tangential intersection angle

(c) Calculation of TIAS

(d) Calculation of JS divergence

Figure 1. The steps to calculate JS divergence of TIAS

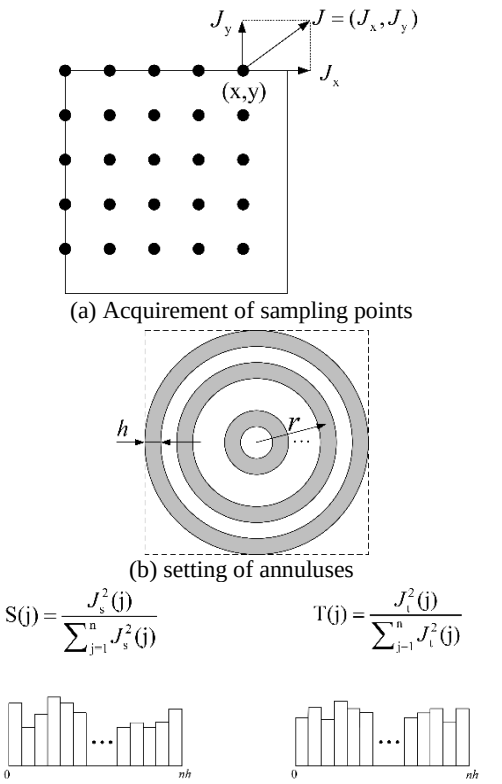

(a) Acquirement of sampling points

(b) setting of annuluses

(c) Calculation of RDES

(d) Calculation of JS divergence

Figure 2. The steps to calculate JS divergence of RDES.

3. FINITE ELEMENT MODELING

In order to extract the EC vectors, the FEMs in allusion to excitation coils were established by COMSOL Multiphysics 5.5. The FEM is composed of three parts: air domain, excitation coil and specimen. Table 1 summarized their main parameters. As is shown in Figure 3(a), there is the FEM of Koch excitation coil under 0.1mm lift-off distance. The element type of the air domain is free tetrahedron mesh. The specimen has two element types. There is a circular area with 10 mm radius on the surface of the specimen, and this field is divided into smaller free triangle mesh. Then, the free triangle mesh is permeated in 1.6 mm far away from the specimen surface by sweeping. Consequently, a column with 1.6 mm high and 10 mm radius is full of the free triangle mesh. The rest element type of the specimen is free tetrahedron mesh. Also, the rest element type of the whole model is free tetrahedron mesh.The mesh of element is shown in Figure 3(b). All of the FEMs are calculated in frequency domain, the set frequencies are 1 kHz, 10 kHz, 20 kHz, 50 kHz, 100 kHz, 200 kHz, 500 kHz, 1000 kHz, 2000 kHz, 5000 kHz and 10000 kHz. In addition, the physics control equations of the FEMs are listed in Equation (10):

$$\begin{cases} \nabla \times \mathbf{H} = \mathbf{J} \\ \mathbf{B} = \nabla \times \mathbf{A} \\ \mathbf{E} = -\mathrm{j}\omega\mathbf{A} \\ \mathbf{J} = \sigma\mathbf{E} + \mathrm{j}\omega\mathbf{D} \end{cases} \tag{10}$$

where $\mathbf{H}$, $\mathbf{J}$, $\mathbf{B}$, $\mathbf{A}$, $\mathbf{E}$ and $\mathbf{D}$ stand for magnetic field, current density, magnetic flux density, magnetic vector potential, electric field, and displacement density, respectively.

TABLE 1. The parameters of FEM

Parameters	Set
Air domain	Dimension: 50 mm ×50 mm×30 mm Relative permeability: 1 Relative permittivity: 1 Conductivity :10 S/m
Koch excitation coil	Diameter of circumcircle: 10 mm (Ideal coil) Edge current: 1 A
Circular excitation coil	Diameter: 10 mm (Ideal coil) Edge current: 1A
Specimen	Aluminum Dimension: 35 mm ×35 mm×6 mm Relative permeability: 1 Relative permittivity: 1 Conductivity :3.774×10^7 S/m

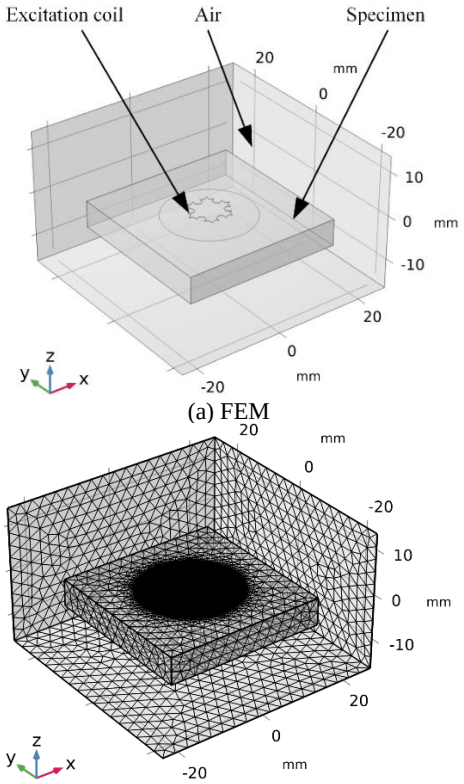

(a) FEM

(b) Meshing

Figure 3. FEM of Koch excitation coil

The boundary condition of the FEMs is magnetic insulation, which is presented as Equation (11):

$$\mathbf{n} \times \mathbf{A} = \mathbf{0} \tag{11}$$

where $\mathbf{n}$ is the vector which is perpendicular to the surface of the air domain.

In addition, to research the correlation between the detectability of the differential pickup probes and the change of EC distributions reflected by JS divergence, the circular differential pickup probe and Koch differential pickup probe were simulated under different lift-off distances. Figure 4 is the FEM of the Koch differential pickup probe for the inspection of the crack. This kind of probe consists of an excitation coil and two pickup coils, and every pickup coil is composed of half of the Koch coil. In addition, the pickup coils are under the excitation coil, and the distance between the pickup coils and the excitation coil is 0.4mm. The tested crack is 3mm in length, 0.25mm in width and 1.6mm in depth. The scanning direction to the crack is 0° and 90°. Compared with Table 1, some parameters are adjusted: the size of air domain is $60\ \mathrm{mm}\times60\ \mathrm{mm}\times30\ \mathrm{mm}$, and the size of specimen is $50\mathrm{mm}\times50\mathrm{mm}\times6\mathrm{mm}$. The element types and meshing method is similar to that of the FEM in Figure 3.

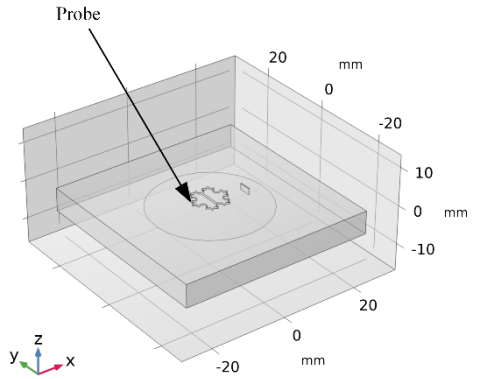

Figure 4. FEM when Koch differential pickup probe inspects crack.

4. EXPERIMENTAL SYSTEM

For the sake of validating the correlation between JS divergence and simulation results of probes relative to crack, the experiment concerned with Koch and circular differential pickup EC probes was carried out. In Figure 5, there is the schematic of the experimental system.

The progress of the experiment can be regarded as two parts: the excitation to signals and the pickup to signals.

The excitation part: firstly, a function generator was used to output signals from two channels. Thereinto, the signal output from channel 1 is a sinusoidal signal whose frequency is 100KHz (excitation frequency) and peak-to-peak value (Vpp) of voltage is 400mV; the signal output from channel 2 is a cosine signal, and its frequency and Vpp are the same as those of channel 1. After that, the signal output from channel 1 flowed into two directions: one passed through a power amplifier and entered into the excitation coil of the probe, the other entered the input end of signal conditioning circuit. In addition, the signal output from channel 2 of the function generator was connected with the input end of the signal conditioning circuit.

The pickup part: this experiment took advantage of the pickup coil on probes to obtain the crack signal detected from a specimen. Then, the signal was demodulated into real part and imaginary part signals. Eventually, the real part and imaginary part signals were gotten via data acquisition card and computer.

To realize the above process, the experimental system was built as shown in Figure 6. The probe was installed on the 3-D scanner and the tested specimen was fixed under the probe. The 3-D scanner was controlled by the computer, which made the probe inspect the pre-crack on the specimen in definite directions. In the experiment, the crack with 3mm in length, 0.25mm in width and 1.6mm in depth was scanned under different lift-off distances (the lift-off distance is set from 0.1mm to 2mm, and the interval is 0.1mm). The directions of scanned crack were set as 0° and 90° which are defined as the angle between scanning direction and crack direction in length, as can be seen in Figure 7.

5. RESULT and DISCUSSION

5. 1. JS Divergence To evaluate the difference of EC distributions between Koch excitation coil and circular excitation coil quantitatively, under different excitation frequencies, the values of JS divergence were calculated at the lift-off distances from 0.1mm and 10.0mm (The interval is 0.1mm from 0.1mm to 2.0mm and 0.5mm from 2.0mm to 10.0mm.)

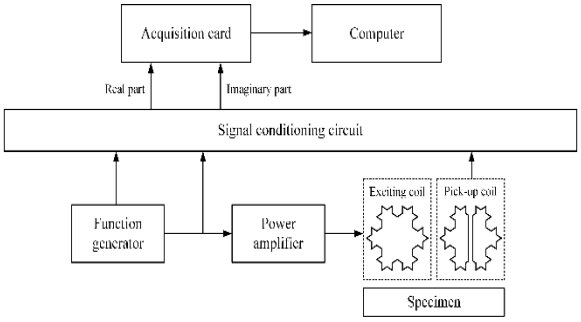

Figure 5. The schematic of experimental system

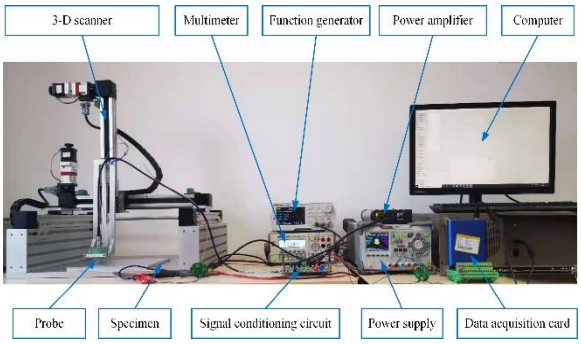

Figure 6. The experimental system

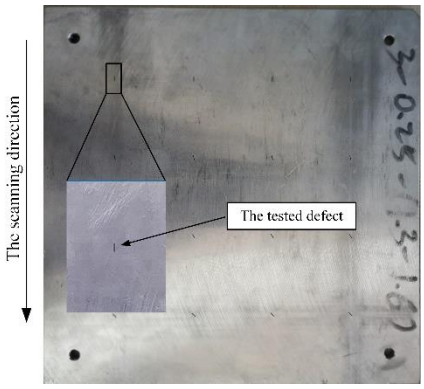

Figure 7. The crack and scanning direction

5. 1. 1. JS Divergence of TIAS Figure 8 shows the values of JS divergence of TIAS. From the perspective of the diversity of EC directions, the result characterizes the difference of EC distributions induced by Koch excitation coil and circular excitation coil under different lift-off distances and excitation frequencies. In general, for each excitation frequency, the value of JS divergence decreases with the increase of the lift-off distance and is close to 0 bit ultimately. In other words, the richness of TIA of EC distribution between the two kinds of coils is getting close. Eventually, the richness is almost identical. When the lift-off distance increases from 0.3 mm to 3.0 mm, the value of JS divergence increases with the increase of the excitation frequency. Therefore, the EC induced by the Koch coil distributes in more directions than the circular coil. When the lift-off distance increases to more than 3 mm, the change of JS divergence is inapparent and close to 0. At this time, the EC distributions between the two kinds of coils are almost identical, and their directions become single. What should be noticed is that the values of JS divergence under 0.1mm, 0.2mm, 0.3mm lift-off distance grows when the excitation frequencies are 500 kHz, 1000 kHz, 2000 kHz, 5000 kHz and 10000 kHz. In addition, there is the maximum value of JS divergence when the excitation frequency is 5000 kHz and the lift-off distance is 0.3 mm. It is illustrated that the EC distributions of Koch excitation coil and circular excitation coil have the biggest difference in the richness of TIA on this occasion.

5. 1. 2. JS Divergence of RDES In Figure 9, there are values of JS divergence based on RDES. Under different lift-off distances and excitation frequencies, the result characterized the difference of EC distributions between Koch excitation coil and circular excitation coil from the view of the EC distribution proportion in each annulus. For each frequency, the value of JS divergence reduces with the increase of the lift-off distance and tends to a horizontal line ultimately. It is illustrated that the ECs induced by Koch coil and circular coil distribute on more and more annuluses. Meanwhile, the EC distribution proportion of the Koch coil in each annulus becomes more and more identical to the EC distribution proportion of the circular coil. When the JS divergence is almost 0 bit, the number of annuluses occupied by the EC induced by the two coils is extremely close to each other. When the lift-off distance is definite, the value of JS divergence increases with the increase of the excitation frequency. It can be inferred that the difference of the number of annuluses occupied by the EC distributions between Koch excitation coil and the circular excitation coil becomes bigger and bigger. In the whole picture, the maximum value of JS divergence exists under 0.1mm lift-off distance and 10000 kHz. At this time, the number of annuluses occupied by the EC distribution induced by the circular coil has the largest difference relative to the number of annuluses occupied by the EC distribution induced by the Koch coil.

5. 2. FEM Simulation Result

5. 2. 1. EC Distributions of Excitation Coil In this section, the difference of EC distributions induced by Koch and circular coils are conveyed intuitively with the increase of the lift-off distance.

As is shown in Figure 10, there are EC distributions induced by Koch excitation coil and circular excitation coil. An obvious Koch-shape EC distribution can be seen in Figure 10(a) when the lift-off distance is 0.1mm. With the increase of lift-off distance, it is increasingly close to a circular EC distribution. Figure 10(b) is the EC distribution under 2.0mm lift-off distance where the Koch shape fades apparently. Figures 10(c) and 10(d) are EC distributions generated by the circular excitation coil when the lift-off distances are 0.1mm and 2.0mm, respectively. The difference of the EC distributions between Figures 10(a) and 10(c) is larger than it between Figures 10(b) and 10(d). The results of JS divergence can illustrate this phenomenon quantitatively.

As can be seen in Figure 11, it shows that the EC distributions when the crack in 0° and 90° directions is

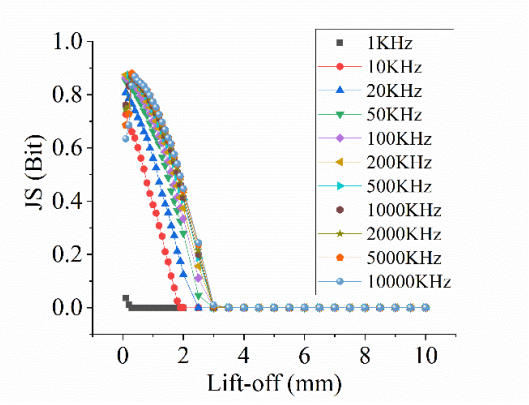

Figure 8. JS of TIAS

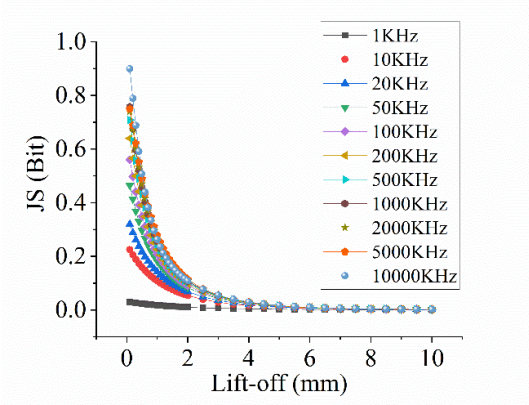

Figure 9. JS of RDES

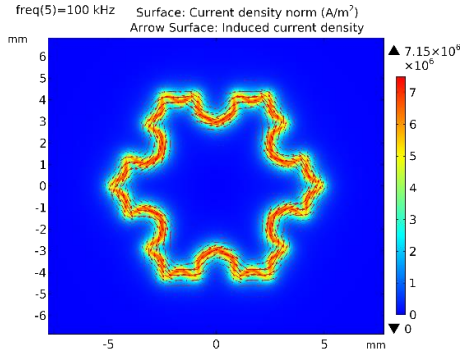

(a) EC distribution of Koch excitation coil under 0.1mm lift-off distance

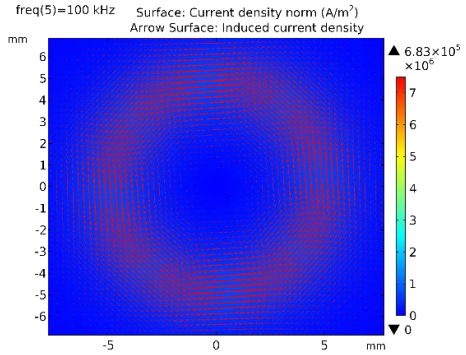

(b) EC distribution of Koch excitation coil under 2.0mm lift-off distance

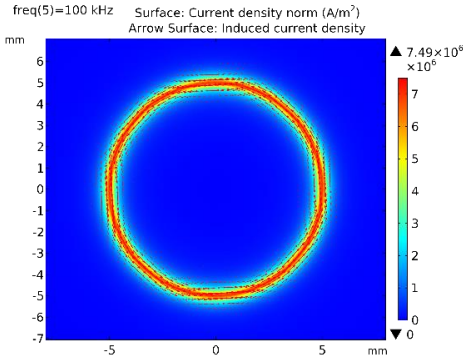

(c) EC distribution of circular excitation coil under 0.1mm lift-off distance

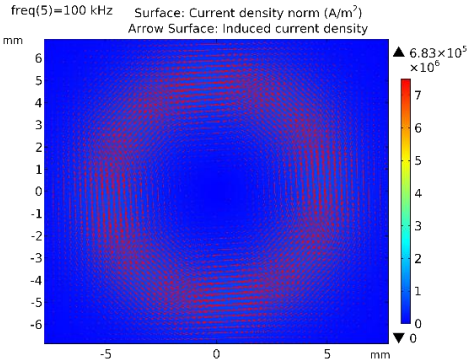

(d) EC distribution of circular excitation coil under 2.0mm lift-off distance

Figure 10. EC distributions of Koch excitation coil and circular excitation coil under 100 kHz

inspected via Koch differential pickup probe. For Koch probe, when the lift-off distance is 0.1mm, the EC induced by its excitation coil distributes in more orientations. Furthermore, the angle between EC vectors and the crack is diverse as shown in Figures 11(a) and 11(b). Conversely, when the lift-off is 2.0mm, the angle between EC vectors and the crack is relatively single as shown in Figures 11(c) and 11(d).

5. 2. 2. Correlation Between the Crack Signals in Two Directions and JS Divergence of TIAS In order to study the detectability of Koch and circular

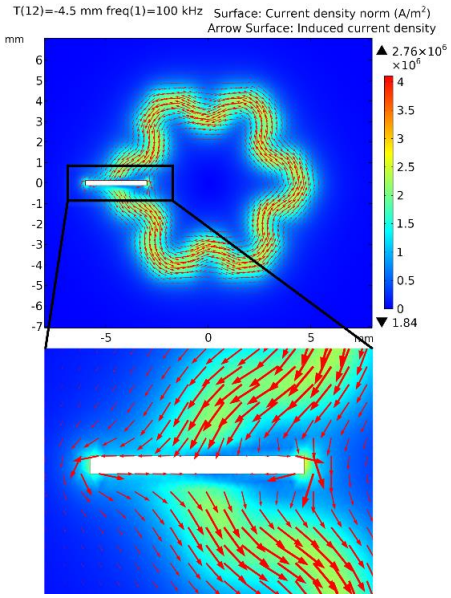

(a) Detection of crack in 0° direction under 0.1 mm lift-off distance

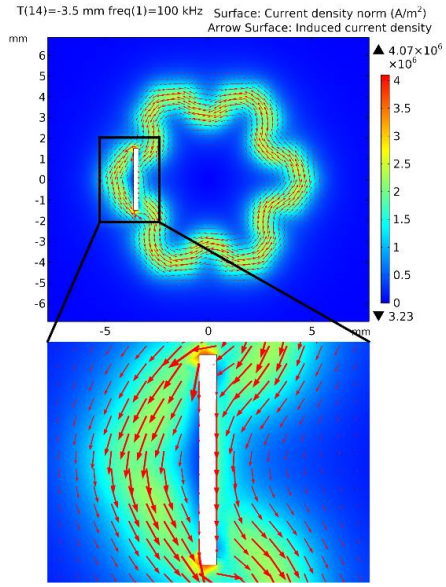

(b) Detection of crack in 90° direction under 0.1 mm lift-off distance

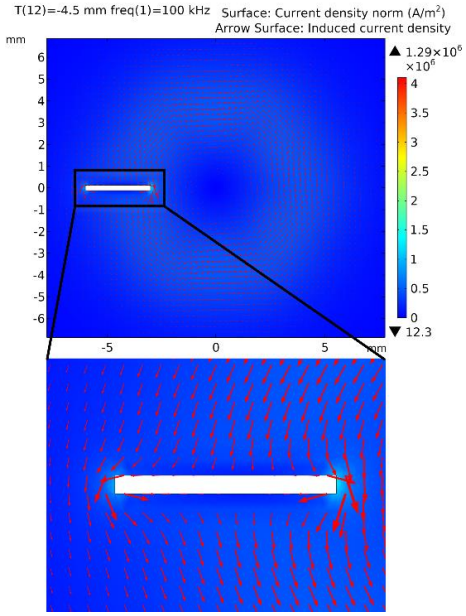

(c) Detection of crack in 0° direction under 2.0 mm lift-off distance

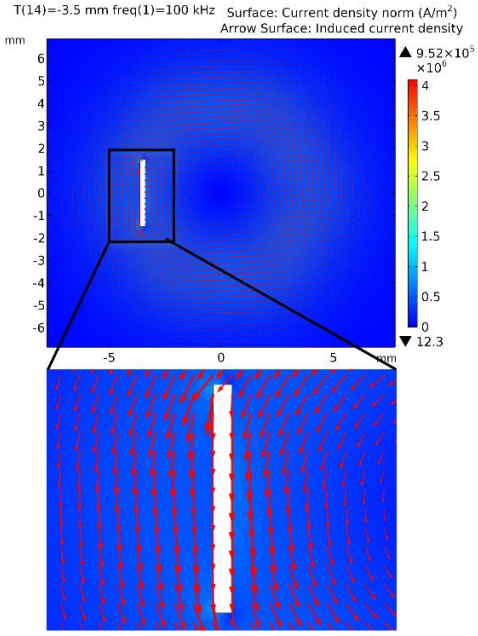

(d) Detection of crack in 90° direction under 2.0 mm lift-off distance

Figure 11. EC distributions of Koch differential pickup probe for the crack detection

pickup probes to the crack in two directions (0° and 90°) and the correlation between the detectability to 90° crack and JS divergence of TIAS, the EC distributions with crack and the rate of relative change of 90° crack to 0° crack are obtained.

Through the same approach to analyze, the inspection of the crack in 0° and 90° directions was carried out by the circular differential pickup probe. As can be seen in Figure 12, there are EC distributions of the circular differential pickup probe for the detection of crack when the lift-off distances are 0.1 mm and 2.0 mm. Although the geometry of circular EC distribution changes not obviously, the angle between the crack and EC vectors becomes more and more monotonous.

In order to research the correlation between the difference of signal in 0° direction and the JS divergence of TIAS, the V_{pp} of signals in 0° and 90° directions were extracted via simulation results with regard to Koch and circular differential pickup probes firstly. Then, the rate

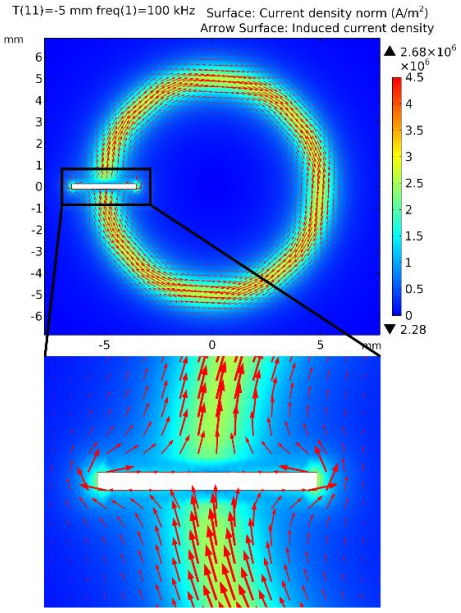

(a) Detection of crack in 0° direction under 0.1 mm lift-off distance

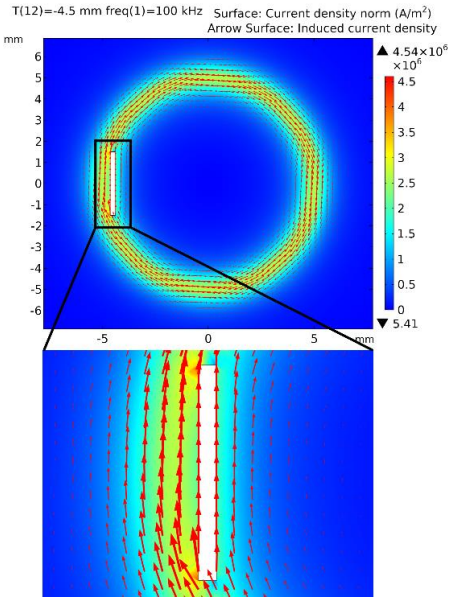

(b) Detection of crack in 90° direction under 0.1 mm lift-off distance

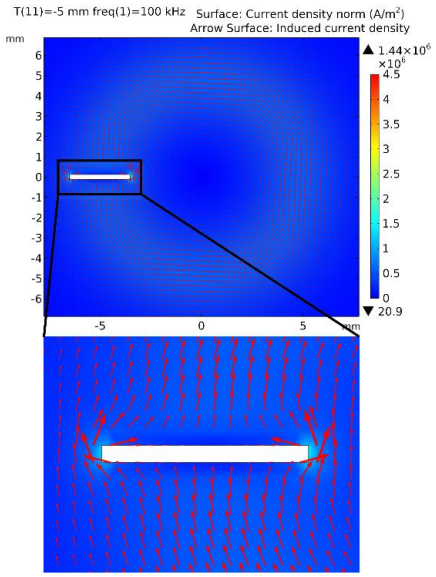

(c) Detection of crack in 0° direction under 2.0 mm lift-off distance

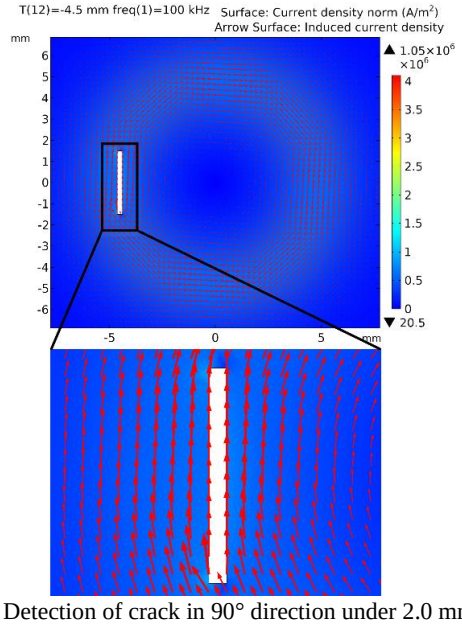

(d) Detection of crack in 90° direction under 2.0 mm lift-off distance

Figure 12. EC distributions of circular differential pickup probe for the crack detection

of relative change of the signal V_{pp} in 90° to the V_{pp} in 0° is calculated by Equation (12):

$$\text{Rate of relative change} = \frac{V_{pp} \text{ of } 0° - V_{pp} \text{ of } 90°}{V_{pp} \text{ of } 0°} \quad (12)$$

By the way, the signals output from the two probes mainly denote the real part signals. As is shown in Figure 13, for the Vpp of signals output from both Koch and circular probes, the rate of relative change increases with the increase of the lift-off distance. It means that the two probes become less and less sensitive for the inspection of the crack in 90° direction relative to the crack in 0° direction. In addition, due to the intrinsic insensitivity of circular probe to the crack in 90° direction, the rates of relative change of circular probe are commonly higher than those of Koch probe. Furthermore, the difference of the rates of relative change of the two probes is smaller and smaller with the increase of the lift-off distance. The reason could be that the EC distributions induced by the two probes get close to each other. Meanwhile, the detectability of both probes to the crack in 90° direction becomes weak with the increase of the lift-off distance.

According to the result of JS divergence of TIAS, with the increase of the lift-off distance, the value of JS divergence is smaller and smaller when the excitation frequency is 100KHz. The TIA of EC distributions generated by Koch and circular probes is more and more monotonous, which contributes rarely to the inspection of the crack in 90° direction. Consequently, the detectability of the two probes is getting closer and closer aimed at the crack in 90° direction, which conforms to the discussion of the previous paragraph.

5. 2. 3. Correlation Between the Width of Crack Signals and JS Divergence of RDES In order to research the correlation between the width of 90° crack signals and JS divergence of RDES, the EC distributions and the output voltages (the voltage of real part signals) of crack detection were obtained by simulation.

Figure 14 shows the EC distributions concerned with the crack detected by Koch and circular differential pickup probes under 0.1mm and 2.0mm lift-off distances. In Figures 14 (a) and 14(b), when the crack passes the edge of EC distributions induced by Koch and circular probes under 0.1mm lift-off distance, due to the different number of annuluses occupied by EC distributions, the signals output from the two probes also have discrimination. At this time, the width of EC distribution determines the area range of interaction between crack

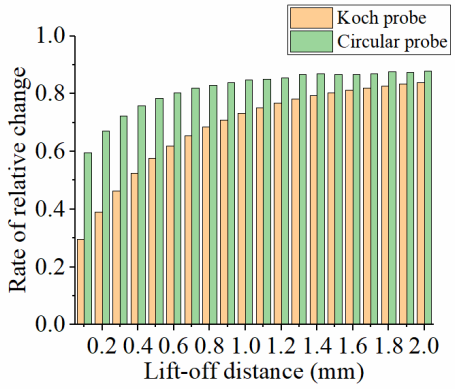

Figure 13. The rate of relative change of the V_{pp} in 90° to the V_{pp} in 0°.

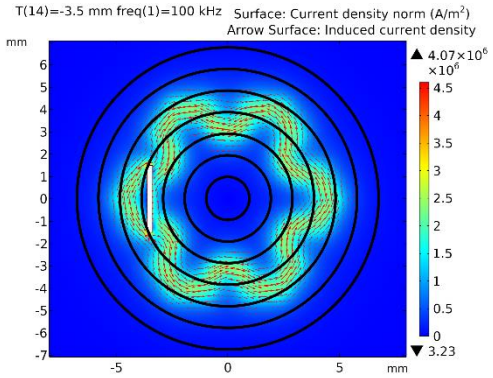

(a) Detection of crack using Koch probe under 0.1 mm lift-off distance

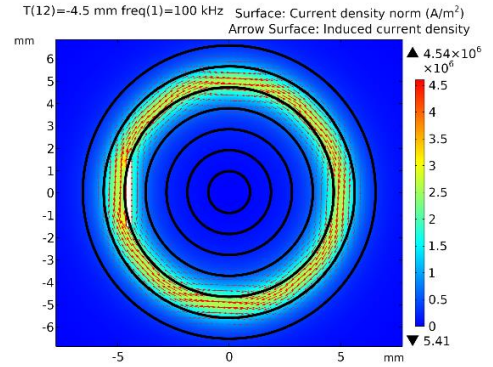

(b) Detection of crack using circular probe under 0.1 mm lift-off distance

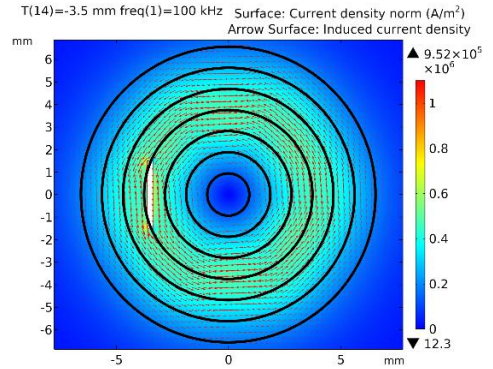

(c) Detection of crack using Koch probe under 2.0 mm lift-off distance

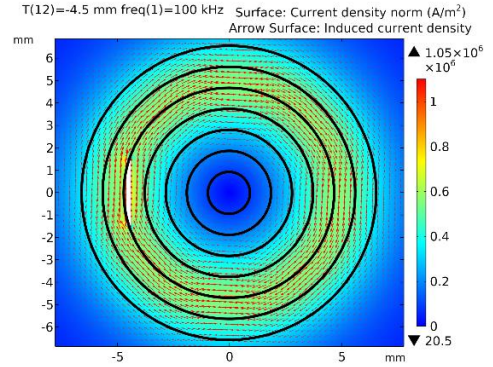

(d) Detection of crack using circular probe under 2.0 mm lift-off distance

Figure 14. EC distributions for the crack detection

and EC. Then, the full width at half maxima (FWHM) of signal namely the width of the signal as shown in Figure 15 was reflected by that. When the lift-off distance increase to 2.0mm as shown in Figures 14 (c) and 14(d), the two EC distributions take up more annuluses correspondingly. Moreover, the area of interaction between crack and EC increases as well.

In order to convey the width of every signal output from the two probes more obviously, the normalization and Gaussian fitting are conducted after getting the signals. In Figure 16, it displays the signals under 0.2mm to 2.0mm lift-off (the step is 0.2mm) distance after normalization and Gaussian fitting. Then, the left FWHM of every signal under every lift-off distance is calculated as the width of the signal. As can be seen in Figure 17, with the increase of lift-off distance, the width of the signal of Koch probe increases at a slow speed, but that of circular probe increases at a relatively fast speed. At the same time, the widths of signals from the two probes are getting close to each other. When the lift-off distance is 2.0mm, the widths of signals of the two probes have little difference.

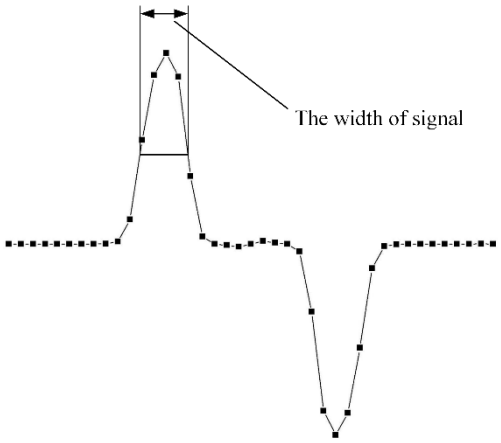

Figure 15. The schematic of the width of signal

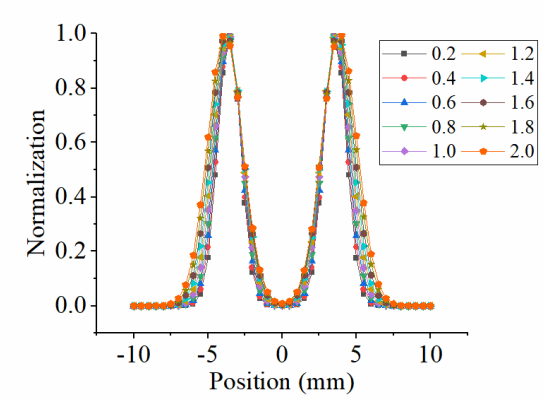

(a) Koch probe

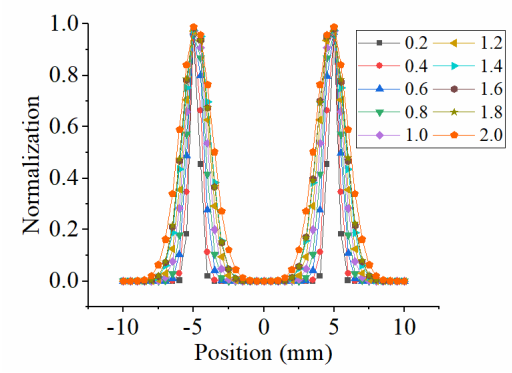

(b) circular probe

Figure 16. The signals after normalization and Gaussian fitting

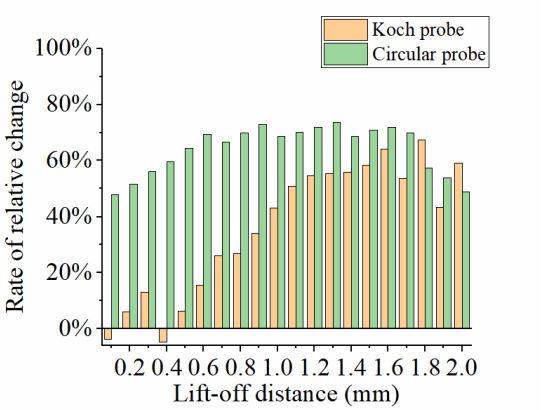

Figure 18. The rate of relative change of the V_{pp} in 90° to the V_{pp} in 0°

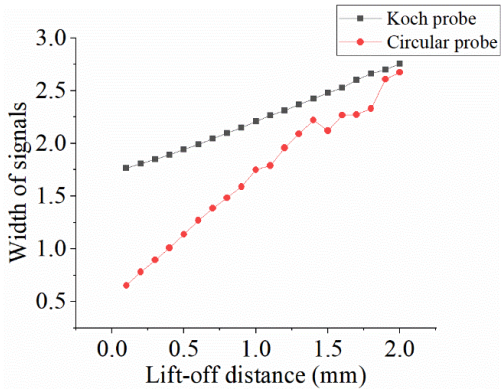

Figure 17. The schematic of the width of signal

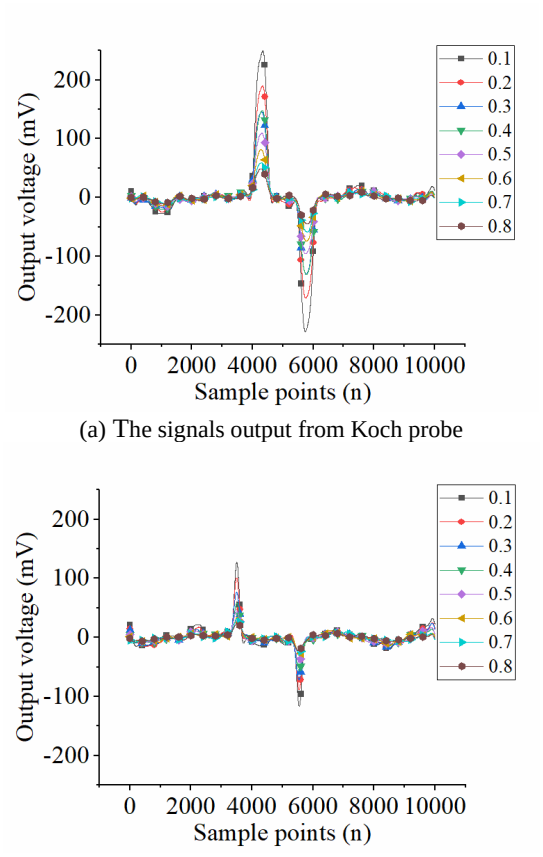

(a) The signals output from Koch probe

(b) The signals output from circular probe

Figure 19. The values of voltage of signals output from two probes

The result can be explicated by the JS divergence of RDES. Because the EC distribution proportion of Koch coil in each annulus becomes more and more identical to the EC distribution proportion of circular coil, the ranges of interaction between the EC induced by the two probes and crack approach to each other. Therefore, it is consistent with the discussion about the widths of signals.

5. 3. Experiment Result In order to validate the simulation result, the experiment about circular and Koch differential pickup probes was carried out.

Figure 18 presents the rates of relative change calculated by Equation (12). Generally speaking, for the Koch probe, although there is fluctuation from 0.1mm to 0.4mm lift-off distance and 1.7mm to 2.0mm distance, the rate of relative change maintains an upward trend when the lift-off distance increases from 0.5mm to 1.6mm. Therefore, it is consistent with the simulation result to some extent. For the circular probe, the tendency of the rates of relative change is consistent with the simulation result under low lift-off distance.

Figure 19 shows the output voltage obtained from the Koch probe and circular probe in the experiment.

Similarly, each signal was processed by normalization and Gaussian fitting. In order to see the width of each signal clearly, the single peak of each signal from the two probes was set in the same range length of sample points (the range of sample points of Koch probe is from 2800 to 4400, and the range of

sample points of the circular probe is from 3400 to 5000) as shown in Figure 20. Then, the left FWHM of every signal is calculated. It can be seen from Figure 21 that the width of signals from the Koch probe is larger than the width from the circular probe when the lift-off distance is small. Meanwhile, with the increase of the lift-off distance, the width of each signal of the circular probe is close to the width of the Koch probe gradually. Therefore, the experiment result is identical to the simulation result.

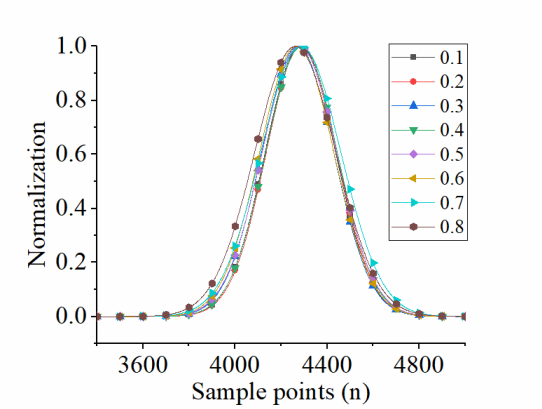

(a) Koch probe

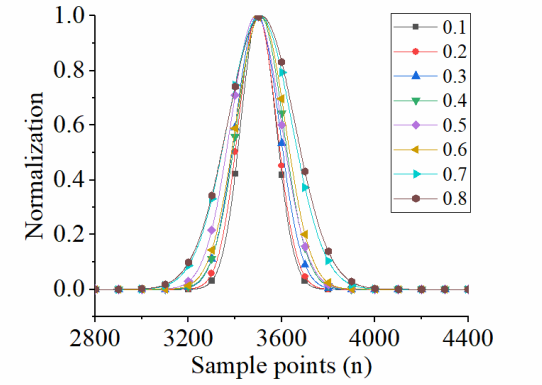

(b) circular probe

Figure 20. The signals after normalization and Gaussian fitting

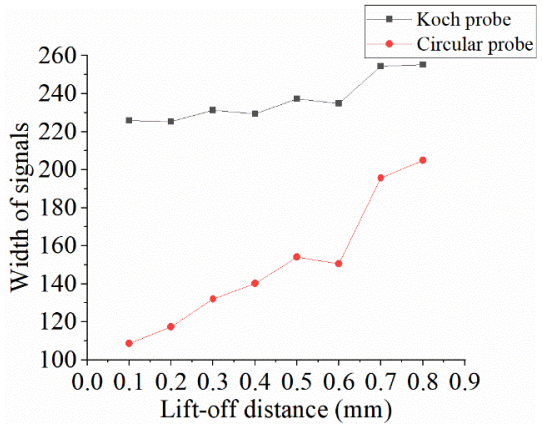

Figure 21. The left FWHM of signals after normalization and Gaussian fitting

6. CONCLUSIONS

In this paper, from the perspective of the diversity of EC orientations and the concentration degree of EC distributions, the JS divergence was applied to evaluate the difference of EC distributions between two different excitation coils. Then, in allusion to the Koch and circular differential pickup probes, the simulation result was conducted to study the correlation between the crack signals and JS divergence. Finally, the experiment was realized to verify the simulation result. It can be concluded that:

(1) In general, with the increase of the lift-off distance and decrease of the excitation frequency, the richness of TIA between Koch coil and circular coil gets close gradually based on the JS divergence of TIAS.

(2) Based on the JS divergence of RDES, with the increase of the lift-off distance and decrease of the excitation frequency, the number of annuluses occupied by the EC distributions induced by Koch and circular coils get close to each other increasingly.

(3) The detectability of Koch and circular differential pickup probes to the crack in 90° direction has a strong correlation with the JS divergence of TIAS to some extent.

(4) The width of crack signals has a relatively strong correlation with the JS divergence of RDES.

7. ACKNOWLEDGE

This work was financially supported by the National Nature Science Foundation of China (Grant No. 51807086 and 12162021), Department of Education of Gansu Province of China (Grant No. 2021QB-047) and the Hongliu youth found of Lanzhou University of Technology.

8. REFERENCES

1. Garcia-Martin, J., Gomez-Gil, J., and Vazquez-Sanchez, E., "Non-destructive techniques based on eddy current testing", ***Sensors***, Vol. 11, (2011), 2525-2565. DOI: 10.3390/s110302525
2. Gilles-Pascaud, C., Decitre, J.M., Vacher, F., Fermon, C., Pannetier, M., and Cattiaux, G., "Eddy current flexible probes for complex geometries", AIP Conference Proceedings, (2006), 399-406. DOI: 10.1063/1.2184556
3. Martinos, J., and Martinos, T., "Experimental development flexible eddy current planar probe", ***Non-Destructive Testing***, (2015), 1-3.

4. Ding, T.H., Chen, X.L., and Huang, Y.P., "Ultra-Thin flexible eddy current sensor array for gap measurements", ***Tsinghua Science and Technology***, Vol. 9, No. 6, (2004), 667-671.
5. Meyendorf, N., Grundy, D., Baaklini, G.Y., Washabaugh, A., Schlicker, D., Michel, B., Shay, I., and Goldfine, N., "Health monitoring using MWM-array and IDED-array sensor networks", ***Advanced Sensor Technologies for Nondestructive Evaluation and Structural Health Monitoring***, Vol. 5770, (2005), 14-23. DOI: 10.1117/12.606069
6. Zilberstein, V., Walrath, K., Grundy, D., Schlicker, D., Goldfine, N., Abramovici, E., and Yentzer, T., "MWM eddy-current arrays for crack initiation and growth monitoring", ***International Journal of Fatigue,*** Vol. 25, (2003), 1147-1155. DOI: 10.1016/j.ijfatigue.2003.08.010
7. Ding, H., He, Y.T., and Jiao, S.B., "Rosette eddy current sensor for structural health monitoring", ***Applied Mechanics and Materials***, Vol. 330, (2013), 430-436. DOI: 10.4028/www.scientific.net/AMM.330.430
8. Fan, X.H., Chen, T., He, Y.T., Du, J.Q., Ma, B.L., and Song, Y.J., "An excitation coil layout method for improving the sensitivity of a rosette flexible eddy current array sensor", ***Smart Materials and Structures***, Vol. 29, (2020), 1-16. DOI: 10.1088/1361-665X/ab5455
9. Sun, Z.G., Cai, D., Zou, C., Zhang, W.Z., and Chen, Q., "A flexible arrayed eddy current sensor for inspection of hollow axle inner surfaces", ***Sensors***, Vol. 16, (2016), 1-9. DOI: 10.3390/s16070952
10. Zhang, H.Y., Ma, L.Y., and Xie, F.Q., "A method of steel ball surface quality inspection based on flexible arrayed eddy current sensor", ***Measurement***, Vol. 144, (2019), 192-202. DOI: 10.1016/j.measurement.2019.05.056
11. Xiao, M., Ju, F., Ning, P., He, Z.Q., Li, K.Y., Zhou, C., and Zhang, Y.Z., "Effects of filler type and aging on self-sensing capacity of cement paste using eddy current-based nondestructive detection", ***Measurement***, Vol. 182, (2021), 1-9. DOI: 10.1016/j.measurement.2021.109708
12. Yin, X.K., Zhang, X.R., Li, Y.Y., Zhu, T., Hutchins, D., Li, W., Chen, G.M., "A combined inductive and capacitive non-destructive evaluation technique using a single spiral coil sensor", ***IEEE Sensors Journal***, Vol. 21, No. 16, (2021), 18187-18195. DOI: 10.1109/JSEN.2021.3084204
13. She, S.B., He, Y.Z., Chen, Y.F., and Chady, T., "Flexible floral eddy current probe for detecting flaws in metal plate", ***IEEE Sensors Journal***, Vol. 20, No. 18, (2020), 10521-10529. DOI: 10.1109/JSEN.2020.2995472
14. She, S.B., Liu, Y.Z., Zhang, S.J., Wen, Z.Z., Zhou, Z.J., Liu, X.K., Sui, Z.H., Ren, D.T., Zhang, F., and He, Y.Z., "Flexible differential butterfly-shape eddy current array sensor for defect detection of screw thread", ***IEEE Sensors Journal***, DOI: 10.1109/JSEN.2021.3093550.
15. Chen, G.L., Cao, Z., and Zhang, W.M., "A novel planar differential Koch fractal eddy current probe with parallel wound topological structure", ***Journal of Sensors***, (2021), 1-13. DOI: 10.1155/2021/6671189
16. Chen, G.L., Zhang, W.M., and Pang, W.H., "Koch curve fractal geometry excitation probe for EC non-destructive testing", ***Measurement***, Vol. 124, (2018), 470-478. DOI: 10.1016/j.measurement.2018.04.031
17. Xie, R.F., Chen, D.X., Pan, M.C., Tian, W.G., Wu, X.Z., Zhou, W.H., and Tang, Y., "Fatigue crack length sizing using a novel flexible eddy current sensor array", ***Sensors***, Vol. 15, (2015) 32138-32151. DOI: 10.3390/s151229911
18. Zhang, W.P., Wang, C.L., Xie, F.Q., and Zhang, H.Y., "Defect imaging curved surface based on flexible eddy current array sensor", ***Measurement***, Vol. 151, (2020), 1-10. DOI: 10.1016/j.measurement.2019.107280
19. Aouf, A., Bouchala, T., Abdou, A., and Abdelhadi, B., "Eddy current probe configuration for full rail top surface inspection", ***Instrumentation Mesure Métrologie***, Vol. 20, No. 2, (2021), 65-72. DOI: 10.18280/i2m.200201
20. Chen, K.F., Gao, B., Tian, G.Y., Yang, Y.P., Yang, C.R., and Ma, Q.P., "Differential coupling double-layer coil for EC testing with high lift-off", ***IEEE Sensors Journal***, Vol. 21, No. 16, (2021), 18146-18155. DOI: 10.1109/JSEN.2021.3076880
21. Fan, X.H., Chen, T., He, Y.T., and Du, J.Q., "Influence of spatial winding distribution of flexible eddy current sensor on quantitative monitoring of subsurface cracks", ***Measurement***, Vol. 178, (2021), 1-15. DOI: 10.1016/j.measurement.2021.109382
22. Zhang, N., Ye, C.F., Peng, L., and Tao, Y., "Eddy current probe with three-phase excitation and integrated array tunnel magnetoresistance sensors", ***IEEE Transactions on Industrial Electronics***, Vol. 68, No. 6, (2021), 5325-5336. DOI: 10.1109/TIE.2020.2989704
23. Chen, G.L., and Cao, Z., "Quantitative evaluation of eddy current distribution by relative entropy and cross entropy", ***Measurement and Control***, Vol. 54, (2021), 1-6. DOI: 10.1177/0020294020984201
24. Zhang, W.M., Chen, G.L., and Pang, W.H., "Shannon information entropy of eddy current density distribution", ***Nondestructive Testing and Evaluation***, Vol. 32, (2016), 152-165. DOI: 10.1080/10589759.2016.1184266
25. Chen, G.L., "Two novel information entropy indices for analysis of the eddy current distribution", ***Entropy***, Vol. 20, (2018), 1-8. DOI: 10.3390/e20090699
26. Chen, G.L., and Zhang, W.M., "Angular spectral density and information entropy for eddy current distribution", ***Entropy***, Vol. 18, (2016), 1-11. DOI: 10.3390/e18110392
27. Lin, J.H., "Divergence measures based on the Shannon entropy", ***IEEE Transactions on Information Theory***, Vol. 37, No. 1, (1991), 145-151. DOI: 10.1109/18.61115

Persian Abstract

چکیده

توزیع جریان گردابی برای عملکرد پروب های جریان گردابی مسطح مهم است. در این مقاله، واگرایی جنسن–شانون طیف زاویه تقاطع مماسی و طیف انرژی جهت شعاعی برای ارزیابی تفاوت بین توزیع‌های جریان گردابی تولید شده توسط کویل‌های محرک دایره‌ای و فراکتالی کوخ پیشنهاد شد. با شبیه سازی برای کویل های محرک دایره ای و کوخ، مشخص می شود که تفاوت توزیع جریان گردابی بین دو نوع کویل با افزایش مقادیر دو واگرایی جنسن–شانون بزرگتر و بزرگتر می شود. در همان زمان، همبستگی بین تغییر واگرایی جنسن–شانون و قابلیت تشخیص ترک کوتاه در جهت خاص از طریق نتایج شبیه‌سازی و آزمایش مورد بحث قرار گرفت. مشخص شد که، نسبت به ترک در جهت ۰ درجه، قابلیت تشخیص پروب‌های پیکاپ دیفرانسیل کوخ و دایره‌ای به ترک در جهت ۹۰ درجه با واگرایی جنسن–شانون طیف زاویه تقاطع مماسی همبستگی دارد. عرض هر سیگنال تولید شده توسط دو پروب با واگرایی جنسن–شانون طیف انرژی جهت شعاعی همبستگی دارد.